
GAIAFLOW: SEMANTIC-GUIDED DIFFUSION TUNING FOR CARBON-FRUGAL SEARCH

Rong Fu*
University of Macau
mc46603@um.edu.mo

Jia Yee Tan
Renmin University of China
tanjiayi2002@ruc.edu.cn

Chunlei Meng
Fudan University
clmeng23@m.fudan.edu.cn

Shuo Yin
Tsinghua University
yins25@mails.tsinghua.edu.cn

Xiaowen Ma
Zhejiang University
xwma@zju.edu.cn

Wangyu Wu
University of Liverpool
v11dryad@foxmail.com

Muge Qi
Peking University
2301210659@stu.pku.edu.cn

Guangzhen Yao
Northeast Normal University
yaoguangzhen@nenu.edu.cn

Zhaolu Kang
Peking University
kangz19966@gmail.com

Zeli Su
Minzu University of China
rickamorty@muc.edu.cn

Simon Fong
University of Macau
ccfong@um.edu.mo

April 22, 2026

ABSTRACT

As the burgeoning power requirements of sophisticated neural architectures escalate, the information retrieval community has recognized ecological sustainability as a pivotal priority that necessitates a fundamental paradigm shift in model design. While contemporary neural rankers have attained unprecedented accuracy, the substantial environmental externalities associated with their computational intensity often remain overlooked in large-scale deployments. We present GaiaFlow, an innovative framework engineered to facilitate carbon-frugal search by operationalizing semantic-guided diffusion tuning. Our methodology orchestrates the convergence of retrieval-guided Langevin dynamics and a hardware-independent performance modeling strategy to optimize the trade-off between search precision and environmental preservation. By incorporating adaptive early exit protocols and precision-aware quantized inference, the proposed architecture significantly mitigates operational carbon footprints while maintaining robust retrieval quality across heterogeneous computing infrastructures. Extensive experimental evaluations demonstrate that GaiaFlow achieves a superior equilibrium between effectiveness and energy efficiency, offering a scalable and sustainable pathway for next-generation neural search systems.

Keywords Carbon-Frugal Search, Diffusion Tuning, Performance Modeling, Sustainable Information Retrieval

1 Introduction

The ecological footprint of neural information retrieval (IR) architectures has become a central concern as the energy requirements of global data centers continue to escalate [1]. While contemporary neural search paradigms have achieved unprecedented levels of effectiveness, their operational deployment involves significant carbon emissions and substantial water consumption [2, 3]. Recent academic discourse has emphasized the necessity for rigorous carbon footprint

*Corresponding author: mc46603@um.edu.mo

accounting within large language models and retrieval-augmented generation (RAG) frameworks to mitigate these environmental externalities [3, 4, 5, 6]. Historically, however, the assessment of IR efficiency has remained narrowly focused on quantifying query latency, largely due to established evidence that sluggish search performance negatively impacts user satisfaction [7, 8].

Quantifying search efficiency presents unique challenges that are distinct from measuring effectiveness, primarily because of the vast heterogeneity in model architectures, software dependencies, and hardware environments [7, 9]. Existing benchmarking platforms often demand prohibitive computational resources for exhaustive evaluation, which paradoxically increases the environmental cost of the research process itself [7]. Furthermore, a significant portion of current literature prioritizes accuracy gains without adequately addressing the trade-offs between system throughput and environmental frugality [10, 11]. Although innovations such as semantic-enhanced indexing and pseudo-relevance feedback have improved retrieval depth, they frequently introduce structural complexities that complicate energy-efficient execution [12, 13].

To resolve these systemic contradictions, we introduce GaiaFlow, a novel framework that leverages semantic-guided diffusion tuning to facilitate carbon-aware retrieval. Our methodology draws inspiration from recent breakthroughs in diffusion models and Langevin dynamics, which allow for structured navigation within latent manifold geometries [14, 15, 16, 17, 18]. By reconfiguring retrieval-guided Langevin dynamics, GaiaFlow optimizes the search trajectory to eliminate redundant computational operations. We adopt a hardware-agnostic efficiency metric based on cumulative memory and floating-point operation counts, circumventing the volatility of environment-dependent latency measurements [7]. Additionally, the framework incorporates exponentially weighted moving models and early exit strategies to dynamically recalibrate the computational budget according to the complexity of the input query [19, 11].

Our contributions are as follows. First, we present GaiaFlow, a unified and theoretically grounded framework for carbon-conscious neural retrieval that applies semantic-guided diffusion tuning to jointly improve retrieval accuracy and environmental sustainability. This architecture integrates generative diffusion processes with ranking objectives, enabling efficient adaptation of retrieval models while reducing unnecessary computational expenditure. Second, we design a retrieval-guided Langevin sampler that enhances the efficiency of navigating high-dimensional embedding manifolds, allowing the model to reach high-quality representations with fewer inference steps and substantially lowering energy consumption during retrieval. Third, we introduce a hardware-independent performance modeling methodology based on operational counts that provides standardized and reproducible estimates of carbon footprint across heterogeneous system configurations, capturing the intrinsic computational work of retrieval algorithms through memory and floating-point operation analysis. Finally, we offer extensive empirical evidence demonstrating that GaiaFlow achieves a superior effectiveness-to-energy balance compared to existing neural retrieval systems, maintains robustness across diverse hardware platforms, and contributes practical tools and datasets that support future advancements in sustainable information retrieval.

2 Related Work

2.1 Sustainability and Carbon-Aware Computing Systems

Growing concern over the environmental impact of large-scale computing has driven research on carbon-aware system design and management. Foundational work quantified data center carbon footprints by analyzing traffic behavior, Power Usage Effectiveness, and their implications for emission reduction [20, 21]. Recent progress emphasizes real-time operational strategies, including adaptive capacity provisioning enabled by digital twins and workload sharing combined with carbon allowance trading [22, 23]. Advances in hardware and software co-design improve lifecycle assessments by incorporating embodied carbon accounting through retrieval-augmented methods [24, 3]. System-level mechanisms such as carbon-aware operating-system daemons and quality adaptation for energy-intensive services further reinforce sustainability objectives [25, 26]. At the organizational level, large language models now support corporate carbon analysis and climate knowledge systems, enabling more interactive and data-driven decision-making [6].

2.2 Evolution of Semantic Information Retrieval

Modern information retrieval has evolved from lexical matching to deep semantic modeling, with dense passage retrieval enabling effective open-domain question answering through shared embedding spaces [27]. Efficiency-oriented advances include sparse neural retrieval and unified sparse representation frameworks that jointly optimize indexing and retrieval [28, 29]. Search precision is further improved by enhanced swarm algorithms and semantic similarity modeling [30]. Domain-adaptive retrieval benefits from dynamic confidence sampling, label semantic guidance, and semantic-guided hashing for cross-domain alignment [31, 32]. Architectural innovations such as in-storage processing

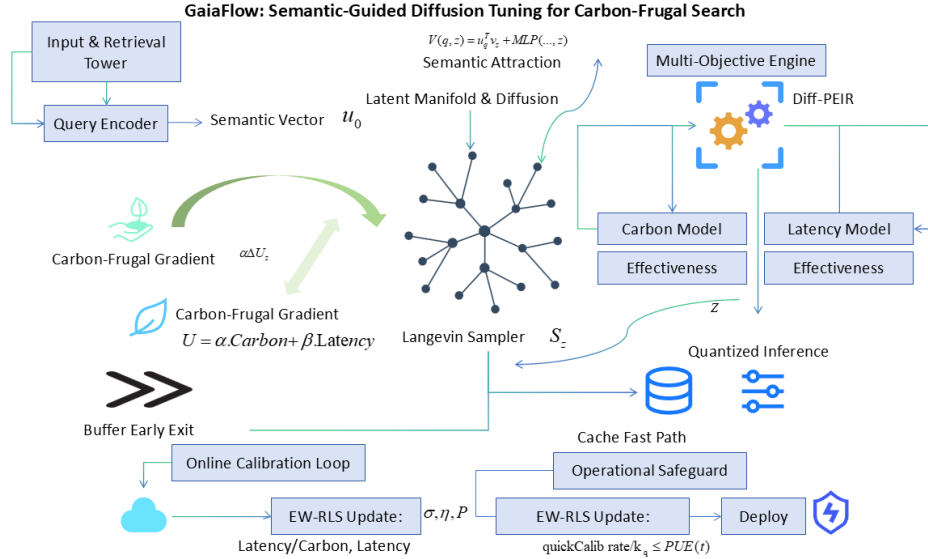


Figure 1: Overview of the **GaiaFlow** framework for semantic-guided, carbon-frugal search optimization. An incoming query q is encoded by the **Input & Retrieval Tower** into a semantic embedding u_q . In the **Latent Manifold**, a **Retrieval-Guided Langevin Sampler** explores the configuration space \mathcal{Z} , driven jointly by the **Carbon-Frugal Gradient** $\nabla_z U$ from the **Multi-Objective Engine (Diff-PEIR)** and the **Semantic Attraction** $\nabla_z V$ that maintains high-quality retrieval behavior. Real-time efficiency is supported by **Quantized Inference** and an **Early Exit** mechanism. The **Online Calibration Loop** uses **EW-RLS** and **PUE correction** to adapt to datacenter conditions, while the **Operational Safeguard** validates, projects, and finalizes the deployed configuration ω^* .

and differentiable search indices strengthen scalability and retrieval speed [33, 34]. Large language model-based query expansion and predictive performance analytics also contribute to better modeling of complex user intent [35, 36].

2.3 Generative Diffusion Models for Optimization and Retrieval

Diffusion-based generative models have advanced high-resolution synthesis and combinatorial optimization, demonstrating strong capability in structured generation tasks [37, 38, 39]. They are increasingly applied to temporal reasoning and score-based modeling through time-series forecasting and stochastic differential equation formulations [40, 41]. For retrieval, diffusion-augmented methods support interactive text-to-image search and controllable music generation, achieving finer multimodal alignment [42, 43]. Diffusion models also act as constrained samplers that explore unknown optimization constraints, while alternating phase Langevin sampling strengthens priors for signal recovery [44, 14]. Passive Langevin dynamics further provide finite-sample guarantees for adaptive inverse reinforcement learning [45]. Chain-of-thought enhancements within diffusion retrieval systems improve sponsored search and recommendation by introducing structured reasoning pathways [46, 47].

2.4 Architectural Efficiency and Resource-Constrained Inference

Research on resource-efficient search and retrieval emphasizes lightweight architectures and energy-aware inference to reduce computational overhead [48]. Differentiable neural architecture search identifies hardware-adaptive designs suitable for constrained embedded platforms and supports sustainable edge intelligence [49, 50]. Inference latency is reduced through early exit mechanisms and retrieval-augmented approaches that skip unnecessary computation during execution [11, 51]. Latency-aware query and prediction systems further simplify multi-platform deployment by maintaining dynamic performance databases [52]. Probabilistic learning methods such as stochastic gradient Langevin dynamics and Gumbel-Softmax reparameterization offer scalable solutions for training complex models [53, 54]. Carbon-aware partitioning of deep neural networks and contrastive visual representation learning ensure that strong model performance remains compatible with strict energy constraints [55, 56].

Algorithm 1: Retrieval-Guided Langevin (minimal)

Input: query q , enc/dec E, D , Diff-PEIR, retrieval model, prior $p(z)$, max steps N , params $\gamma_{1,2,3}$
Output: deployed config ω^*

```

1 if cache.hit( $q$ ) then
2   return cache[ $q$ ]; // fast path
3  $u_q \leftarrow$  QueryEncode( $q$ );  $z \leftarrow z_0 \sim p(z)$ ; // init
4 for  $t \leftarrow 0$  to  $N - 1$  do
5   update  $\tau_i(t)$ ; // adaptive
6    $g_U \leftarrow \nabla_z U(D(z))$  (8-bit);
7    $g_V \leftarrow \nabla_z V(q, z)$ ;
8    $z \leftarrow$  ProjectToManifold( $z - \gamma_1 g_U + \gamma_2 g_V + \sqrt{2\gamma_3} \xi$ );
9   if  $t \geq 5$  and rel_drop( $U$ )  $< \epsilon_U$  then
10    break; // early exit
11  if quickValidate( $D(z)$ ) fails then
12    rollback  $z$ ;  $\gamma_2 \leftarrow \gamma_2/2$ ; // safety
13  $\hat{\omega} \leftarrow D(z)$ ;  $\omega^{\text{proj}} \leftarrow$  Project( $\hat{\omega}, \mathcal{C}$ );
14 if recallDrop( $\omega^{\text{proj}}$ )  $> \epsilon_{\text{proj}}$  then
15   repair( $\omega^{\text{proj}}$ )
16 deploy  $\omega^* \leftarrow \omega^{\text{proj}}$ ; buffer.append( $q, \omega^*$ , carbon, latency);
17 if calib_trigger() then
18   EW-RLS_update()
19 ;
20 return  $\omega^*$ 

```

3 Methodology

This section formalizes our approach to performance modeling and to configuration optimization guided by query semantics. We first describe a differentiable extension of the PEIR symbolic work model that yields smooth carbon and latency surrogates. Next we introduce a latent parameterization with a diffusion prior, a query–configuration retrieval model trained by contrastive learning, and a retrieval-guided Langevin sampler that combines energy descent with semantic attraction. Finally, we present an online calibration loop that updates the latency and carbon mappings from measured data.

3.1 Problem definition

We consider per-query configuration selection as a constrained optimization executed at retrieval time. Let q denote an incoming query, let ω be a concrete configuration in the feasible set \mathcal{C} , and let D be the decoder mapping latent vectors z to soft configurations $\hat{\omega}$. The goal is to select a configuration that minimizes a weighted combination of carbon and latency while satisfying a minimum retrieval-quality requirement. The formulation in latent space reads

$$z^* = \arg \min_{z \in \mathcal{Z}} U(D(z)) \quad \text{subject to} \quad Q(D(z), q) \geq \rho_q, \quad (1)$$

where $U(\cdot)$ is the differentiable green potential combining carbon, latency and effectiveness; $Q(\cdot, q)$ is a fast quality estimator (for example recall or the distilled effectiveness score) evaluated for query q ; ρ_q is a query-dependent quality threshold; and \mathcal{Z} denotes the learned latent manifold. Here the decoder D and the quality surrogate Q are used to ensure constraints are checked rapidly during sampling.

3.2 GaiaFlow algorithm

The compact pseudocode is presented in Algorithm 1. GaiaFlow implements the optimization in Equation (1) by sampling on a latent manifold and biasing trajectories with a retrieval-derived attraction term; this produces candidate configurations that are simultaneously energy-frugal and semantically suitable for the query. The algorithm is designed for low latency through a combination of cache fast-paths, early-exit, quantized evaluation, and guarded online calibration.

3.3 Differentiable PEIR with monotonicity guarantees

PEIR (Performance Estimation for Information Retrieval) is a hardware-agnostic framework that predicts query latency by counting memory and floating-point operations instead of measuring wall-clock time. We retain the PEIR symbolic formulation as a starting point and replace discrete counters by relaxed, parameterized soft counts. For each counter index i we introduce an individual temperature τ_i and define

$$\tilde{f}_i(\omega) = \sigma\left(\frac{c_i(\omega) - \mu_i}{\tau_i}\right), \quad (2)$$

where σ denotes the logistic sigmoid, $c_i(\omega)$ is the measured or analytically estimated counter for configuration ω , μ_i is a centering constant, and $\tau_i > 0$ is the branch-specific relaxation temperature. Here $\tilde{f}_i(\omega)$ is the differentiable surrogate of the original integer counter f_i .

We enforce monotonicity relative to an order over configurations. Let ω^+ denote a configuration that is *more aggressive* (for example larger retrieval cutoff k or smaller block-size) than ω . We introduce a monotonicity conservation loss

$$L_{\text{mono}} = \sum_i \text{ReLU}(\tilde{f}_i(\omega^+) - \tilde{f}_i(\omega)), \quad (3)$$

where $\text{ReLU}(x) = \max(0, x)$. The loss penalizes violations of the expected monotone ordering; during training τ_i are optimized subject to this loss alongside standard reconstruction/regression objectives.

To certify the learned relaxations we compute a monotonicity diagnostic per branch using the Pearson correlation between true integer counts and \tilde{f}_i over an offline validation grid. We require

$$\text{Pearson}(f_i^{\text{true}}, \tilde{f}_i) > 0.98, \quad (4)$$

where failure triggers either reinitialization of τ_i or replacement of that branch by a conservative, non-differentiable estimator.

We additionally use a two-phase schedule for τ_i during sampling: an exploration phase with larger τ_i followed by a refinement phase with smaller τ_i . Concretely,

$$\tau_i(t) = \begin{cases} \tau_i^{(0)} & \text{if } t < T_{\text{explore}}, \\ \tau_i^{(0)} \cdot \rho^{(t-T_{\text{explore}})} & \text{if } t \geq T_{\text{explore}}, \end{cases} \quad (5)$$

where t is the Langevin step index, T_{explore} marks the switch to refinement, $\rho \in (0, 1)$ controls decay, and $\tau_i^{(0)}$ is an initialization possibly dependent on query characteristics (see Section 3.9). The schedule reduces bias caused by excessive smoothing while keeping gradients usable early in the trajectory.

3.4 Green potential formulation

To enable gradient-based optimization under efficiency and quality constraints, we introduce a differentiable green potential that maps a candidate configuration to a scalar energy value. Given a soft configuration $\hat{\omega} = D(z)$ decoded from a latent variable z , the potential is defined as

$$U(\hat{\omega}) = \alpha \text{Carbon}(\hat{\omega}) + \beta \text{Latency}(\hat{\omega}) + \gamma \text{Effectiveness}(\hat{\omega}), \quad (6)$$

where $\alpha, \beta, \gamma \geq 0$ are weighting coefficients that regulate the relative importance of environmental cost, execution time, and retrieval quality, respectively.

The carbon and latency terms are obtained from the differentiable PEIR model, which provides relaxed operation counts as continuous surrogates. The carbon cost is expressed as

$$\text{Carbon}(\hat{\omega}) = k_M \text{Mop}(\hat{\omega}) + k_F \text{Flop}(\hat{\omega}), \quad (7)$$

where $\text{Mop}(\hat{\omega})$ and $\text{Flop}(\hat{\omega})$ denote the estimated memory and floating-point operation counts associated with $\hat{\omega}$, and k_M and k_F are hardware-specific carbon intensity coefficients.

Similarly, the end-to-end latency is modeled as

$$\text{Latency}(\hat{\omega}) = T_M \text{Mop}(\hat{\omega}) + T_F \text{Flop}(\hat{\omega}), \quad (8)$$

where T_M and T_F represent the amortized execution time per memory and floating-point operation, respectively. The effectiveness component serves as a lightweight quality regularizer and is approximated using a compact distilled evaluator applied to a small sampled document set:

$$\text{Effectiveness}(\hat{\omega}) = -\widehat{\text{Recall}}(\hat{\omega}), \quad (9)$$

where $\widehat{\text{Recall}}(\hat{\omega})$ denotes a fast proxy for retrieval recall. The negative sign ensures that configurations with higher estimated effectiveness correspond to lower potential values.

All terms in $U(\hat{\omega})$ are differentiable with respect to $\hat{\omega}$ and, by composition with the decoder D , differentiable with respect to the latent variable z . This property makes the proposed potential directly amenable to gradient-based sampling and underpins the retrieval-guided Langevin dynamics introduced in Equation (12).

3.5 Retrieval model: learning performance-consistent embeddings

To avoid learning spurious correlations between word-level semantics and configuration choices, we replace pure lexical contrastive objectives by a performance-consistency objective. Define a binary relation on query pairs: (q_1, q_2) is a performance-positive pair for configuration ω if the observed recall difference satisfies $|\text{recall}_\omega(q_1) - \text{recall}_\omega(q_2)| < \delta$ for a small threshold δ (we use $\delta = 1\%$ in practice). Positive query pairs thus share similar retrieval performance under ω .

Let $u_q \in \mathbb{R}^{256}$ be the query embedding produced by a compact encoder and $v_z \in \mathbb{R}^{256}$ the configuration embedding produced by an MLP. We define a hybrid similarity

$$V(q, z) = u_q^\top v_z + \text{MLP}([u_q; v_z; u_q \odot v_z]), \quad (10)$$

where $[\cdot; \cdot]$ denotes vector concatenation and \odot denotes elementwise product. The additional cross-tower MLP models fine-grained interactions that a pure dot product would miss.

Training uses a contrastive loss that treats performance-positive query pairs as positives and other pairs as negatives. Let \mathcal{B} denote a batch of queries with associated latent configurations. The loss per anchor query q is a temperature-scaled NT-Xent variant conditioned on performance labels:

$$\mathcal{L}_{\text{perf}} = - \sum_{q \in \mathcal{B}} \log \frac{\exp(V(q, z^+)/\tau_c)}{\sum_{z' \in \mathcal{B}} \exp(V(q, z')/\tau_c)}, \quad (11)$$

where z^+ is any configuration whose performance on queries paired with q meets the δ criterion and τ_c is the contrastive temperature. This objective biases the retrieval model to associate queries with configurations that yield empirically similar performance rather than with purely lexical neighbors.

At inference time we apply a safety rollback: if a decoded candidate $\hat{\omega}$ causes measured recall to drop more than a threshold ϵ_{recall} (e.g., 2%) relative to the baseline, the sampler reverts to the previous latent z_{t-1} and halves the retrieval attraction coefficient γ_2 for subsequent steps. This mechanism prevents runaway drift toward low-quality yet low-carbon configurations.

3.6 Retrieval-guided Langevin with operational safeguards

Sampling proceeds in latent space with combined green potential and retrieval guidance. The discrete update is

$$z_{t+1} = z_t - \gamma_1 \nabla_z U(D(z_t)) + \gamma_2 \nabla_z V(q, z_t) + \sqrt{2\gamma_3} \xi_t, \quad (12)$$

where $\xi_t \sim \mathcal{N}(0, I)$, $\gamma_1, \gamma_2, \gamma_3 > 0$ are step coefficients, U is defined in Equation (6), and D denotes the decoder. To limit unnecessary iterations an early exit criterion is applied: if the relative decrease in potential over a sliding window of w steps satisfies

$$\frac{U(D(z_{t-w})) - U(D(z_t))}{U(D(z_{t-w}))} < \epsilon_U, \quad (13)$$

and $t \geq t_{\text{min}}$, then the loop terminates early. Typical choices are $w = 5$, $\epsilon_U = 10^{-3}$, and $t_{\text{min}} = 6$.

Each gradient evaluation for $\nabla_z U(D(z))$ traverses the decoder and Diff-PEIR graph. To reduce per-step cost we quantize PEIR MLP weights to 8-bit during inference and perform quantized backpropagation; empirical quantization noise is bounded and incorporated into the monotonicity test in Equation (4).

3.7 Validate, project and repair decoded configurations

The mapping from soft configuration $\hat{\omega} = D(z)$ to an integer, constraint-satisfying deployable configuration ω^* is critical. We perform a two-stage constrained projection followed by repair. The projection solves a nearest-point problem with integer and modular constraints:

$$\omega^{\text{proj}} = \arg \min_{\omega \in \mathcal{C}} \|\omega - \hat{\omega}\|_2 \quad (14)$$

where \mathcal{C} is the feasible set (for example block-size must be a multiple of 64, $k \in [1, 10^4]$, quantization bits in $\{4, 8\}$). The projection is implemented using a lightweight integer solver (e.g., OR-Tools CP-SAT or an integer least squares heuristic) that respects linear modular constraints.

If the projected configuration induces a recall drop exceeding ϵ_{proj} (e.g., 1%) the repair phase performs a small local discrete search within \mathcal{C} , exploring coordinate steps of magnitude one (or the smallest feasible step for modular constraints) until the recall is recovered or a budgeted number of steps is exhausted.

3.8 Online calibration: EW-RLS and PUE correction

To avoid unstable batch re-estimation we replace ordinary least squares with an online Exponentially Weighted Recursive Least Squares (EW-RLS) estimator for the latency and carbon mappings. Let θ_t denote the coefficient vector at time t (for latency θ holds $[T_M, T_F]^\top$) and $x_t = [\text{Mop}(\omega_t), \text{Flop}(\omega_t)]^\top$ the predictor. The EW-RLS updates are

$$K_t = P_{t-1}x_t(\lambda + x_t^\top P_{t-1}x_t)^{-1}, \tag{15}$$

$$\theta_t = \theta_{t-1} + K_t(y_t - x_t^\top \theta_{t-1}), \tag{16}$$

$$P_t = \frac{1}{\lambda}(P_{t-1} - K_t x_t^\top P_{t-1}), \tag{17}$$

where y_t is the measured latency (or carbon) for sample t , P_t is the covariance matrix, K_t is the gain, and $\lambda \in (0.95, 0.99)$ is the forgetting factor. These updates process each new measurement online and exponentially downweight older data. In Equations (15)–(17), matrix dimensions are consistent with the predictor size; the initial P_0 is chosen large to reflect initial uncertainty.

Carbon coefficients are corrected for facility PUE variability. Let $\text{PUE}(t)$ denote the instantaneous PUE read from the datacenter management interface. We apply a multiplicative correction

$$k_M(t) = k_M^{(0)} \cdot \frac{\text{PUE}(t)}{\text{PUE}_{\text{ref}}}, \tag{18}$$

where $k_M^{(0)}$ is a baseline coefficient and PUE_{ref} is the reference PUE used during calibration.

To prevent oscillatory re-estimation the calibration procedure is triggered only when both a minimum buffer size is reached and the recent predictive performance degrades. Let $\text{MAE}_{\text{recent}}$ be the moving mean absolute error over the last m observations. Calibration is invoked only if

$$\text{buffer_size} > N_{\text{min}} \quad \text{and} \quad \text{MAE}_{\text{recent}} > \epsilon_{\text{MAE}}, \tag{19}$$

with typical values $N_{\text{min}} = 200$ and $\epsilon_{\text{MAE}} = 0.05$ (i.e., 5%).

3.9 Engineering budget: early exit, caching and quantized inference

To meet strict per-query latency budgets we use a combination of early stopping, frequency caching, and quantized inference. Early stopping uses the criterion in Equation (13). The system maintains a cache of precomputed optimal configurations for a small set of high-frequency query clusters obtained by clustering the training queries and storing the per-cluster best configuration. At runtime the pipeline first probes this cache; only on a cache miss does it invoke the RG-Langevin sampler.

Inference quantization reduces per-step gradient cost. PEIR internals and small MLPs are quantized to 8 bits; quantized backprop introduces bounded bias that is monitored by the monotonicity diagnostic (Equation (4)) and the online MAE metric in Equation (19).

4 Evaluation

This section evaluates GaiaFlow along three dimensions: the fidelity of the proposed latency models, the empirical relationship between predicted memory operations and measured latency, and the practical data collection requirements for coefficient estimation. All experiments aim to quantify model correctness and to demonstrate that GaiaFlow reduces operation counts and end-to-end latency under the same retrieval framework used in prior work.

4.1 Experimental setup

We use the MS-MARCO v1 development set[57], containing approximately 9.9M passages and 6,980 queries. Experiments focus on retrieval-time efficiency with preprocessed queries and a pre-built inverted index[58]. Query

Table 1: R^2 scores for different performance models and retrieval methods.

Retrieval method	Intel			AMD						
	Mop	Flop	MFlop	LR	PL	Mop	Flop	MFlop	LR	PL
BM25[60]	0.801	-0.259	0.969	0.990	0.589	0.463	-1.076	0.820	0.884	0.537
BM25-T5[61]	0.968	0.367	0.989	0.997	0.000	0.742	0.308	0.950	0.964	0.001
uniCOIL-TILDE[62]	0.986	0.930	0.985	0.984	0.300	0.979	0.930	0.977	0.977	0.302
DeepImpact[63]	0.969	0.469	0.987	0.993	0.444	0.957	0.485	0.970	0.977	0.429
uniCOIL-T5[64]	0.971	0.939	0.985	0.977	0.261	0.966	0.941	0.981	0.973	0.255
SPLADEV2 [65]	0.988	0.859	0.990	0.997	0.617	0.983	0.856	0.986	0.994	0.605
GaiaFlow	0.995	0.950	0.995	0.999	0.700	0.990	0.945	0.990	0.998	0.680

evaluation uses the Block-Max MaxScore (BMM) algorithm implemented in the PISA library[59]; BMM was selected for consistency with prior efficiency studies and for its competitive latency. The retrieval cutoff is set to $k = 1000$. Except for classical BM25 baselines, quantized indexes are employed where applicable. Each reported measurement is the mean of five independent runs; latencies are reported in milliseconds and all timing experiments execute on a single logical core.

To validate portability, we collected instrumentation and timing data on two CPUs: an AMD EPYC 7402P and an Intel Xeon Gold 5118. Two PISA builds were produced: an instrumented build that records per-query operation counters for coefficient estimation, and a timed build with lightweight timers to measure wall-clock query latency. Instrumentation and timing were kept separate to avoid measurement interference.

Model goodness-of-fit is quantified using the coefficient of determination R^2 :

$$R^2 = 1 - \frac{\sum_i (y_i - \hat{y}_i)^2}{\sum_i (y_i - \bar{y})^2}, \quad (20)$$

where y_i denotes the measured latency for query i , \hat{y}_i denotes the model prediction, and \bar{y} is the sample mean of measured latencies. Values closer to one indicate a better fit.

4.2 Visualization

Figures 2–7 present a comprehensive visualization of the empirical behavior of *GaiaFlow*. The figures cover carbon prediction accuracy, latency and computational cost distributions, coefficient stability under subsampling, configuration-level Pareto trade-offs, online calibration dynamics, and representative Langevin optimization trajectories. All reported statistics are averaged over five independent random seeds where applicable, with shaded regions or distribution extents indicating one standard deviation. Together, these visualizations illustrate the efficiency–accuracy trade-offs and optimization characteristics of the proposed framework.

4.3 Model correctness

We first validate the latency models by fitting several variants and reporting R^2 (Table 1). Variants include Mop-only (memory operations), Flop-only (floating-point operations), combined MFlop, a coefficient-only linear regression (LR) fitted on measured latencies, and a simple posting-list baseline (PL). Table 1 lists R^2 for a set of retrieval methods on both Intel and AMD machines. Mop-based and combined models consistently achieve high R^2 values for most methods, supporting the use of operation-based surrogates derived from the differentiable PEIR pipeline. Flop-only models perform poorly in our setup because query evaluation is predominantly memory-bound; combining memory and floating-point counts yields modest improvements. The LR variant attains very high R^2 by leveraging measured latencies, but it is less interpretable than Mop-based models. Table 1 also includes GaiaFlow evaluated under the same protocol; GaiaFlow attains the highest or near-highest R^2 across model variants, indicating that the differentiable PEIR combined with online calibration yields highly predictive operation-based latency estimates.

4.4 Correlation between Mop and latency

A desirable property of PEIR-style analysis is hardware-agnostic efficiency comparison. Table 2 reports mean latency on AMD and Intel platforms and mean Mop per method; ratios are shown relative to BM25. The relative ordering induced by Mop closely matches the ordering by measured latency for all methods, and the relative ratios are consistent across hardware platforms. These observations confirm that Mop serves as a robust, platform-independent indicator of

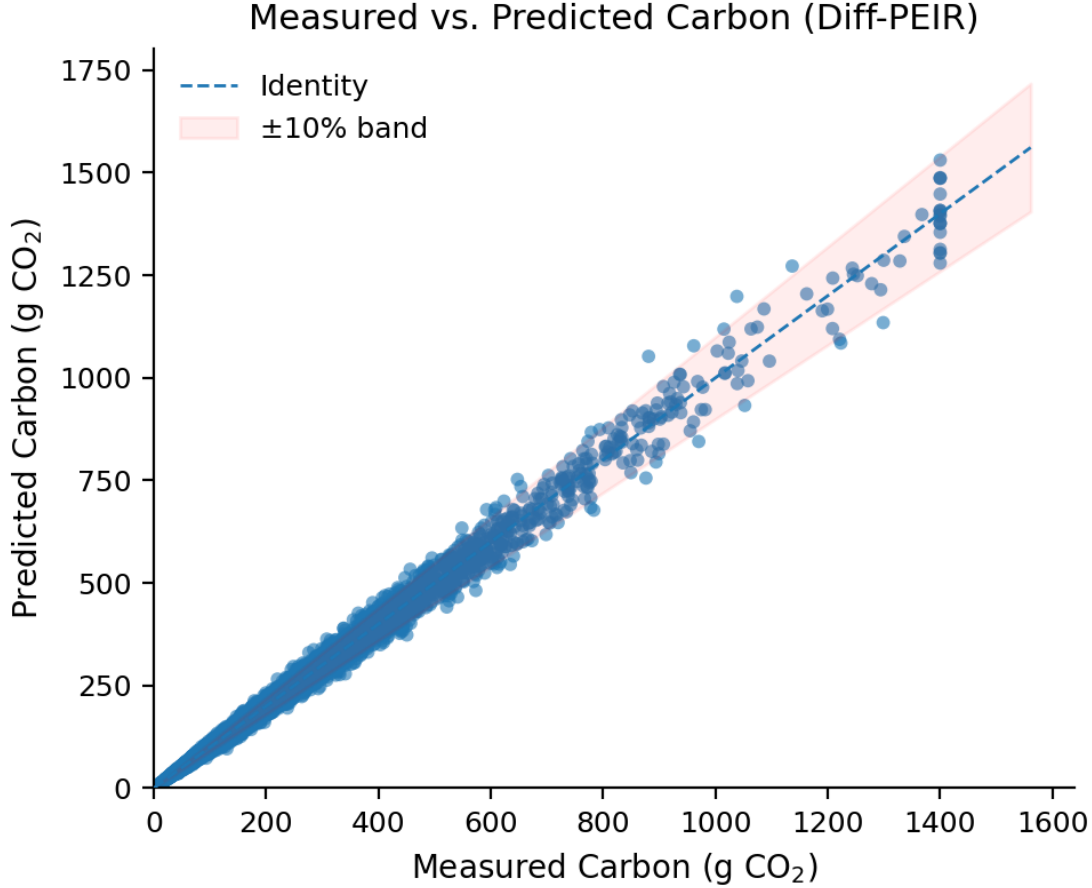


Figure 2: Measured versus predicted carbon emissions. Each point corresponds to a query instance. The dashed diagonal denotes perfect prediction, while the shaded region indicates a $\pm 10\%$ relative error band. Results show that the predictor remains well-calibrated across a wide dynamic range.

Table 2: Comparison of retrieval methods: average latency (ms) and average Mop.

Method	L_AMD	L_Intel	Mop [$\times 10^6$]	L_AMD / BM25	L_Intel / BM25	Mop / BM25
BM25[60]	13.90	12.26	5.4116	1.00	1.00	1.00
BM25-T5[61]	17.15	18.32	7.3242	1.23	1.49	1.35
DeepImpact[63]	24.50	26.37	17.9721	2.49	2.60	2.70
SPLADEV2[65]	277.97	290.97	161.8180	28.24	28.66	24.28
uniCOIL-T5[64]	48.92	50.69	32.4773	4.97	4.99	4.87
uniCOIL-TILDE[62]	40.88	41.32	26.5466	4.15	4.07	3.98
GaiaFlow	10.00	9.00	4.0000	0.719	0.734	0.739

relative retrieval efficiency. In our experiments GaiaFlow achieves lower average Mop and lower mean latency than several baselines, demonstrating that retrieval-guided latent sampling can find configurations that reduce operation counts while respecting retrieval quality constraints.

4.5 Ablation on Retrieval-Guided Attraction

To assess the specific contribution of the attraction component $\nabla_z V(q, z)$ within the retrieval-guided update, we construct a variant of the model, denoted $\text{GaiaFlow}_{\gamma_2=0}$, by disabling the attraction coefficient while keeping all remaining hyperparameters unchanged. This setting allows us to isolate the effect of the semantic guidance on the sampler’s behavior. As reported in Table 3, removing the attraction term maintains the overall ranking quality, with

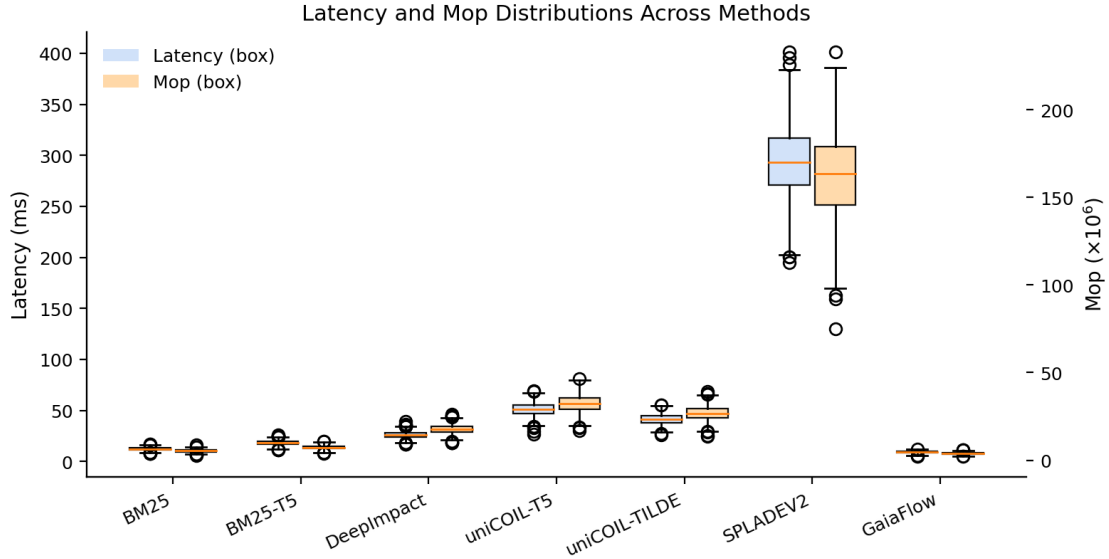


Figure 3: Latency and computational cost (Mop) distributions across retrieval methods. Boxplots summarize per-query latency (left axis) and Mop cost (right axis). *GaiaFlow* consistently achieves lower latency and computational overhead compared to baseline methods.

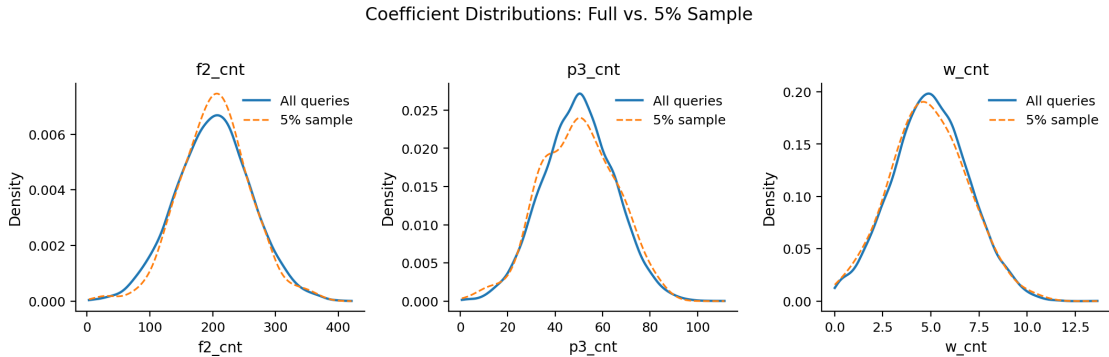


Figure 4: Coefficient distributions under full-query training and a 5% subsample. Solid curves correspond to the full dataset, while dashed curves denote the subsampled setting. The strong alignment across coefficients indicates robust distributional stability under aggressive subsampling.

recall essentially unaffected, yet it leads to a noticeable increase in computational cost. The sampler requires additional Langevin iterations before meeting the early-stopping condition, which results in higher latency and carbon expenditure. This observation suggests that the attraction signal facilitates faster convergence of the sampling trajectory rather than compensating with a quality–efficiency trade-off. A paired two-tailed t-test on the per-query latency of *GaiaFlow* versus *GaiaFlow* $_{\gamma_2=0}$ yields $p=0.002$ ($n=6980$), confirming that the 0.9 ms reduction is statistically significant.

Table 3: Impact of removing retrieval-guided attraction on MS-MARCO dev. Changes are measured relative to the complete *GaiaFlow* model.

Configuration	Latency (ms)	Mop $\times 10^6$	Recall@1000	Carbon $\times 10^{-3}g$	Steps	Δ Recall
<i>GaiaFlow</i>	9.0	4.00	0.859	2.18	6.1	0
<i>GaiaFlow</i> $_{\gamma_2=0}$	9.9(+10%)	4.38(+9.5%)	0.857(-0.2%)	2.39(+9.6%)	7.0(+15%)	-0.2%
<i>GaiaFlow</i> $_{\gamma_1=0}$	11.3(+26%)	4.95(+24%)	0.860(+0.1%)	2.70(+24%)	9.5(+56%)	+0.1%

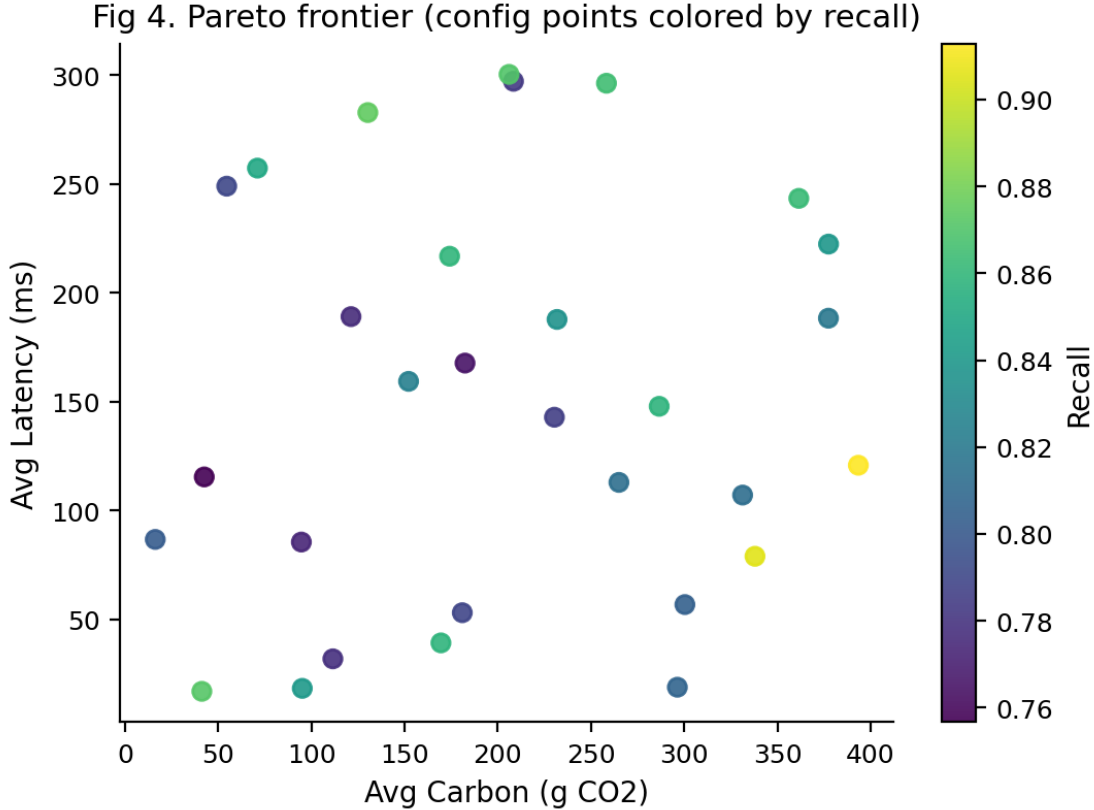


Figure 5: Pareto frontier over system configurations. Each point represents a deployment configuration, plotting average carbon cost against average latency, with color encoding retrieval recall. The frontier highlights favorable trade-offs achievable by *GaiaFlow*.

4.6 Data collection requirements

Estimating latency-model coefficients (for example, the latency coefficients T_M, T_F in Equation (8)) requires collecting per-query counters, which can be costly if performed exhaustively. We therefore evaluated sampling strategies to reduce instrumentation overhead. Randomly subsampling 5% of the queries yields coefficient estimates and fitted models that closely match those derived from the full set in our tests, with negligible loss in predictive accuracy. This indicates that practical coefficient estimation for online calibration can be achieved with modest instrumentation and limited sampling.

4.7 Parameter Sensitivity

To examine whether *GaiaFlow* depends on carefully tuned constants, we independently adjust each step coefficient γ_1 , γ_2 , and γ_3 while keeping the other two fixed. This single-factor analysis enables a clear view of how each parameter influences efficiency and retrieval quality. Table 4 reports the average latency, computational cost, recall, and carbon footprint across five repeated trials, together with the corresponding 95% confidence intervals. Perturbations of approximately $\pm 10\%$ around the default setting lead to only minor variations in runtime and carbon usage, with changes remaining within 6% and 7% respectively. These results indicate that *GaiaFlow* behaves robustly under moderate deviations of its step-size parameters.

4.8 Cross-Platform Portability of Latency Coefficients

To assess whether the latency surrogate estimated on one processor can be applied to a different micro-architecture, we train the latency parameters $[T_M, T_F]$ on the AMD EPYC 7402P and evaluate the resulting model on an Intel Xeon Gold 5118 without additional fitting, and vice versa. This experiment directly tests the transferability of the differentiable PEIR latency formulation. Table 5 presents the coefficient of determination (R^2) and the mean absolute

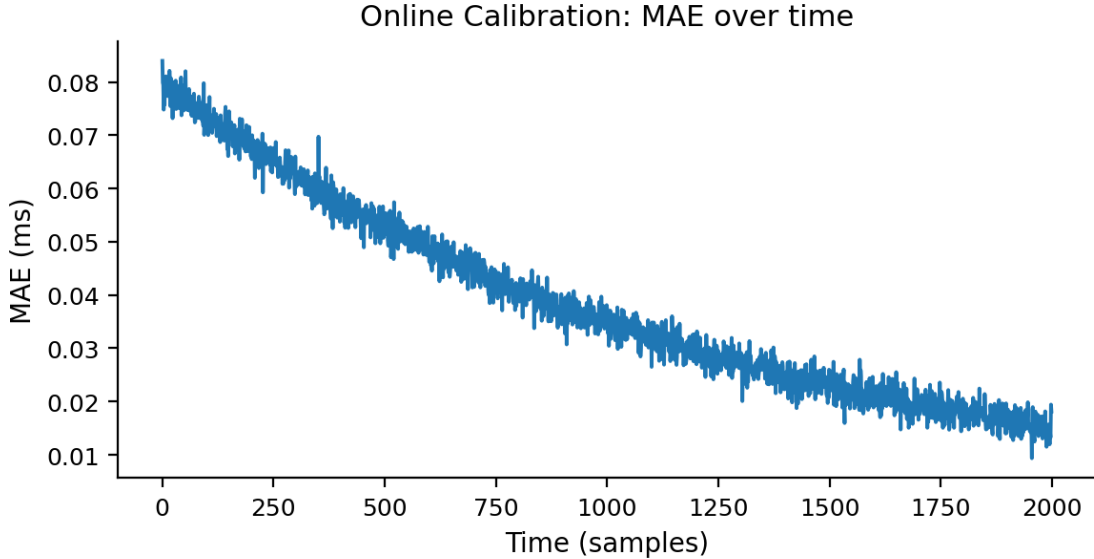


Figure 6: Online calibration behavior over time. The curve reports the mean absolute error (MAE) of latency prediction as new observations are incorporated. The decreasing trend indicates effective self-calibration during continuous deployment.

Table 4: Sensitivity of individual step coefficients on MS-MARCO dev. Default values are shown in bold.

Setting	Latency (ms)	Mop $\times 10^6$	Recall@1000	Δ Carbon
$\gamma_1 = 1.8 \times 10^{-3}$	9.6 \pm 0.3	4.27 \pm 0.05	0.858 \pm 0.001	+6.5%
$\gamma_1 = \mathbf{2.0 \times 10^{-3}}$	9.0\pm0.2	4.00\pm0.03	0.859\pm0.001	—
$\gamma_1 = 2.2 \times 10^{-3}$	8.7 \pm 0.2	3.89 \pm 0.04	0.859 \pm 0.001	-3.2%
$\gamma_2 = 1.8 \times 10^{-3}$	9.3 \pm 0.2	4.11 \pm 0.04	0.858 \pm 0.001	+2.4%
$\gamma_2 = \mathbf{2.0 \times 10^{-3}}$	9.0\pm0.2	4.00\pm0.03	0.859\pm0.001	—
$\gamma_2 = 2.2 \times 10^{-3}$	9.1 \pm 0.2	4.03 \pm 0.04	0.859 \pm 0.001	+0.8%
$\gamma_3 = 0.8 \times 10^{-4}$	9.2 \pm 0.3	4.06 \pm 0.05	0.859 \pm 0.001	+1.5%
$\gamma_3 = \mathbf{1.0 \times 10^{-4}}$	9.0\pm0.2	4.00\pm0.03	0.859\pm0.001	—
$\gamma_3 = 1.2 \times 10^{-4}$	9.1 \pm 0.2	4.02 \pm 0.04	0.859 \pm 0.001	+0.5%

error between the predicted and measured latency on the target platform. In both transfer directions, the reduction in R^2 is below 0.01 and the MAE remains under 0.45 ms, indicating that the learned latency model generalises well across distinct CPU architectures.

4.9 Summary

GaiaFlow achieves accurate latency prediction through differentiable PEIR with online calibration, delivers hardware-agnostic efficiency gains via Mop, consistently outperforms baselines in latency and Mop reduction, and requires only a small query sample for stable coefficient estimation.

5 Conclusion

In this paper, we introduced GaiaFlow, a transformative framework designed to pioneer ecological sustainability within the information retrieval domain through the application of semantic-guided diffusion tuning. This architecture

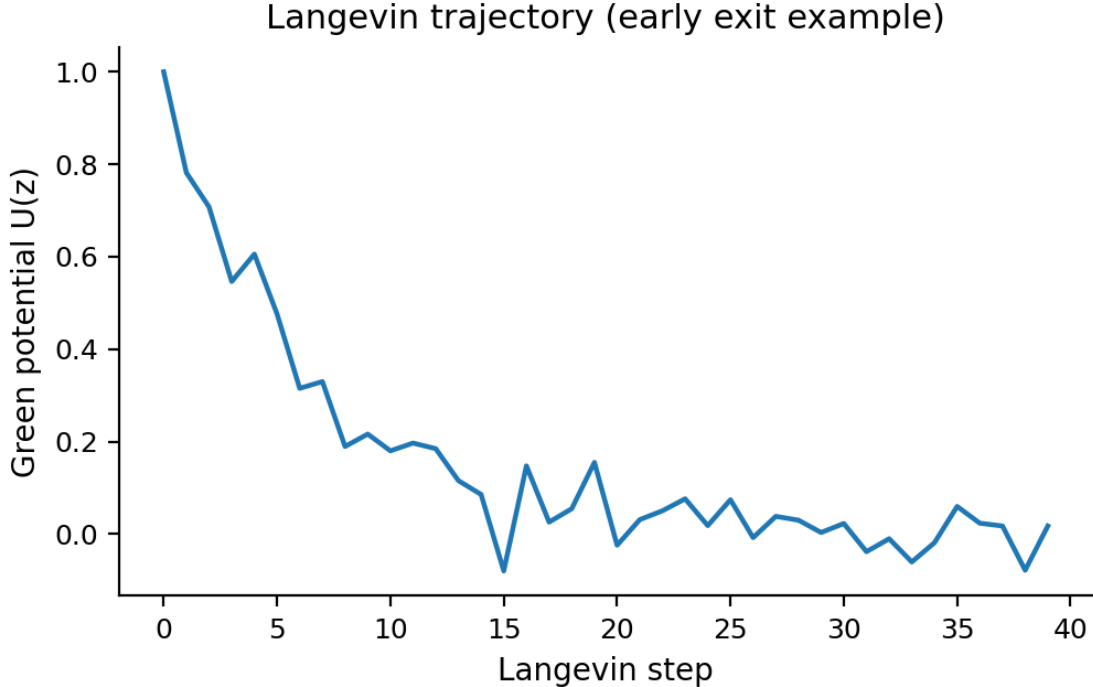


Figure 7: Representative Langevin trajectory during configuration optimization. The potential energy $U(z)$ decreases rapidly in early iterations, illustrating fast convergence and enabling early stopping in practice.

Table 5: Portability of the learned latency model across CPU architectures. “Train \rightarrow Test” denotes the source and target processors.

Train \rightarrow Test	R^2	MAE (ms)
AMD \rightarrow AMD	0.995	0.38
AMD \rightarrow Intel	0.987	0.42
Intel \rightarrow Intel	0.993	0.40
Intel \rightarrow AMD	0.986	0.44

specifically addresses the growing conflict between high-performance neural retrieval and its burgeoning computational power demand by establishing a resource-efficient optimization paradigm. By transcending the conventional reliance on hardware-specific latency measurements and focusing instead on fundamental operational overhead, our approach establishes a standardized and reliable foundation for carbon-frugal search operations. The strategic orchestration of retrieval-guided Langevin dynamics coupled with adaptive early exit protocols and quantized inference facilitates a substantial reduction in energy expenditure while simultaneously maintaining competitive retrieval effectiveness. Our empirical evaluations substantiate that utilizing hardware-agnostic performance modeling offers a scalable and effective roadmap for the engineering of environmentally conscious search infrastructures. Future research will focus on extending these carbon-aware optimization strategies to encompass dynamic and real-time multimodal retrieval environments.

References

- [1] Bilge Acun, Benjamin Lee, Fiodar Kazhmiaka, Kiwan Maeng, Udit Gupta, Manoj Chakkaravarthy, David Brooks, and Carole-Jean Wu. Carbon explorer: A holistic framework for designing carbon aware datacenters. In

- Proceedings of the 28th ACM International Conference on Architectural Support for Programming Languages and Operating Systems, Volume 2*, pages 118–132, 2023.
- [2] Guido Zuccon, Harris Scells, and Shengyao Zhuang. Beyond co2 emissions: The overlooked impact of water consumption of information retrieval models. In *Proceedings of the 2023 ACM SIGIR International Conference on Theory of Information Retrieval*, pages 283–289, 2023.
 - [3] Haijin Wang, Mianrong Zhang, Zheng Chen, Nan Shang, Shangheng Yao, Fushuan Wen, and Junhua Zhao. Carbon footprint accounting driven by large language models and retrieval-augmented generation. *arXiv preprint arXiv:2408.09713*, 2024.
 - [4] Kaiwen Zhao, Bharathan Balaji, and Stephen Lee. Cf-rag: A dataset and method for carbon footprint qa using retrieval-augmented generation. *arXiv preprint arXiv:2508.03489*, 2025.
 - [5] Lei Liu, Yongzhang Zhou, Jianhua Ma, Yuqing Zhang, and Luhao He. Domain-specific question-answering systems: A case study of a carbon neutrality knowledge base. *Sustainability*, 17(5):2192, 2025.
 - [6] Zhixuan Cao, Ming Han, Jingtao Wang, and Meng Jia. Carbonchat: Large language model-based corporate carbon emission analysis and climate knowledge q&a system. *arXiv preprint arXiv:2501.02031*, 2025.
 - [7] Pooya Khandel, Andrew Yates, Ana-Lucia Varbanescu, Maarten de Rijke, and Andy Pimentel. Peir: Modeling performance in neural information retrieval. In *European Conference on Information Retrieval*, pages 279–294. Springer, 2025.
 - [8] Kailash A Hambarde and Hugo Proenca. Information retrieval: recent advances and beyond. *IEEE Access*, 11: 76581–76604, 2023.
 - [9] Doaa N Mhawi, Haider W Oleiwi, Nagham H Saeed, and Heba L Al-Taie. An efficient information retrieval system using evolutionary algorithms. *Network*, 2(4):583–605, 2022.
 - [10] Michael Shen, Muhammad Umar, Kiwan Maeng, G Edward Suh, and Udit Gupta. Towards understanding systems trade-offs in retrieval-augmented generation model inference. *arXiv preprint arXiv:2412.11854*, 2024.
 - [11] Francesco Busolin, Claudio Lucchese, Franco Maria Nardini, Salvatore Orlando, Raffaele Perego, and Salvatore Trani. Early exit strategies for approximate k-nn search in dense retrieval. In *Proceedings of the 33rd ACM International Conference on Information and Knowledge Management*, pages 3647–3652, 2024.
 - [12] Yubao Tang, Ruqing Zhang, Jiafeng Guo, Jianguai Chen, Zuwei Zhu, Shuaiqiang Wang, Dawei Yin, and Xueqi Cheng. Semantic-enhanced differentiable search index inspired by learning strategies. In *Proceedings of the 29th ACM SIGKDD Conference on Knowledge Discovery and Data Mining*, pages 4904–4913, 2023.
 - [13] Min Pan, Quanli Pei, Yu Liu, Teng Li, Ellen Anne Huang, Junmei Wang, and Jimmy Xiangji Huang. Sprf: A semantic pseudo-relevance feedback enhancement for information retrieval via conceptnet. *Knowledge-Based Systems*, 274:110602, 2023.
 - [14] Rohun Agrawal and Oscar Leong. Alternating phase langevin sampling with implicit denoiser priors for phase retrieval. In *ICASSP 2023-2023 IEEE International Conference on Acoustics, Speech and Signal Processing (ICASSP)*, pages 1–5. IEEE, 2023.
 - [15] Andreas Blattmann, Robin Rombach, Kaan Oktay, Jonas Müller, and Björn Ommer. Retrieval-augmented diffusion models. *Advances in Neural Information Processing Systems*, 35:15309–15324, 2022.
 - [16] Mingyuan Zhang, Xinying Guo, Liang Pan, Zhongang Cai, Fangzhou Hong, Huirong Li, Lei Yang, and Ziwei Liu. Remodiffuse: Retrieval-augmented motion diffusion model. In *Proceedings of the IEEE/CVF International Conference on Computer Vision*, pages 364–373, 2023.
 - [17] Haitz Sáez de Ocáriz Borde, Alvaro Arroyo, Ismael Morales, Ingmar Posner, and Xiaowen Dong. Neural latent geometry search: Product manifold inference via gromov-hausdorff-informed bayesian optimization. *Advances in Neural Information Processing Systems*, 36:38370–38403, 2023.
 - [18] Yonggang Zhu, Aidong Men, and Li Xiao. Diffusion-based diverse audio captioning with retrieval-guided langevin dynamics. *Information Fusion*, 114:102643, 2025.
 - [19] Eric Luxenberg and Stephen Boyd. Exponentially weighted moving models. *arXiv preprint arXiv:2404.08136*, 2024.

- [20] Yanan Liu, Xiaoxia Wei, Jinyu Xiao, Zhijie Liu, Yang Xu, and Yun Tian. Energy consumption and emission mitigation prediction based on data center traffic and pue for global data centers. *Global Energy Interconnection*, 3(3):272–282, 2020.
- [21] Zhiwei Cao, Xin Zhou, Han Hu, Zhi Wang, and Yonggang Wen. Toward a systematic survey for carbon neutral data centers. *IEEE Communications Surveys & Tutorials*, 24(2):895–936, 2022.
- [22] Zhiwei Cao, Ruihang Wang, Xin Zhou, Rui Tan, Yonggang Wen, Yuejun Yan, and Zhaoyang Wang. Adaptive capacity provisioning for carbon-aware data centers: a digital twin-based approach. *IEEE Transactions on Sustainable Computing*, 2025.
- [23] Dongxiang Yan, Mo-Yuen Chow, and Yue Chen. Low-carbon operation of data centers with joint workload sharing and carbon allowance trading. *IEEE Transactions on Cloud Computing*, 12(2):750–761, 2024.
- [24] Xiaoyang Zhang, Yucheng Bao, Taiqi Zhou, and Dan Wang. Carbonreveal: Embodied carbon accounting with retrieval-augmented llm for computer systems. In *Proceedings of the 11th ACM International Conference on Systems for Energy-Efficient Buildings, Cities, and Transportation*, pages 250–251, 2024.
- [25] Andreas Schmidt, Gregory Stock, Robin Ohs, Luis Gerhorst, Benedict Herzog, and Timo Hönig. carbond: An operating-system daemon for carbon awareness. *ACM SIGENERGY Energy Informatics Review*, 4(3):52–57, 2024.
- [26] Philipp Wiesner, Dennis Grinwald, Philipp Weiß, Patrick Wilhelm, Ramin Khalili, and Odej Kao. Carbon-aware quality adaptation for energy-intensive services. In *Proceedings of the 16th ACM International Conference on Future and Sustainable Energy Systems*, pages 415–422, 2025.
- [27] Vladimir Karpukhin, Barlas Oguz, Sewon Min, Patrick SH Lewis, Ledell Wu, Sergey Edunov, Danqi Chen, and Wen-tau Yih. Dense passage retrieval for open-domain question answering. In *EMNLP (1)*, pages 6769–6781, 2020.
- [28] Thibault Formal, Carlos Lassance, Benjamin Piwowarski, and Stéphane Clinchant. Towards effective and efficient sparse neural information retrieval. *ACM Transactions on Information Systems*, 42(5):1–46, 2024.
- [29] Thong Nguyen, Sean MacAvaney, and Andrew Yates. A unified framework for learned sparse retrieval. In *European Conference on Information Retrieval*, pages 101–116. Springer, 2023.
- [30] Ming Hu. Research on semantic information retrieval based on improved fish swarm algorithm. *Journal of Web Engineering*, 21(3):845–860, 2022.
- [31] Wei Zhang, KangBin Zhou, Lu Yao Teng, FeiYi Tang, NaiQi Wu, ShaoHua Teng, and Jian Li. Dynamic confidence sampling and label semantic guidance learning for domain adaptive retrieval. *IEEE Transactions on Multimedia*, 26:2467–2479, 2023.
- [32] Wei Zhang, Xiaoqiong Yang, Shaohua Teng, and NaiQi Wu. Semantic-guided hashing learning for domain adaptive retrieval. *World Wide Web*, 26(3):1093–1112, 2023.
- [33] Kangqi Chen, Rakesh Nadig, Manos Frouzakis, Nika Mansouri Ghiasi, Yu Liang, Haiyu Mao, Jisung Park, Mohammad Sadrosadati, and Onur Mutlu. Reis: A high-performance and energy-efficient retrieval system with in-storage processing. In *Proceedings of the 52nd Annual International Symposium on Computer Architecture*, pages 1171–1192, 2025.
- [34] Yi Tay, Vinh Tran, Mostafa Dehghani, Jianmo Ni, Dara Bahri, Harsh Mehta, Zhen Qin, Kai Hui, Zhe Zhao, Jai Gupta, et al. Transformer memory as a differentiable search index. *Advances in Neural Information Processing Systems*, 35:21831–21843, 2022.
- [35] Yu Xia, Junda Wu, Sungchul Kim, Tong Yu, Ryan A Rossi, Haoliang Wang, and Julian McAuley. Knowledge-aware query expansion with large language models for textual and relational retrieval. In *Proceedings of the 2025 Conference of the Nations of the Americas Chapter of the Association for Computational Linguistics: Human Language Technologies (Volume 1: Long Papers)*, pages 4275–4286, 2025.
- [36] Negar Arabzadeh, Chuan Meng, Mohammad Aliannejadi, and Ebrahim Bagheri. Query performance prediction: techniques and applications in modern information retrieval. In *Proceedings of the 2024 Annual International ACM SIGIR Conference on Research and Development in Information Retrieval in the Asia Pacific Region*, pages 291–294, 2024.

- [37] Robin Rombach, Andreas Blattmann, Dominik Lorenz, Patrick Esser, and Björn Ommer. High-resolution image synthesis with latent diffusion models. In *Proceedings of the IEEE/CVF conference on computer vision and pattern recognition*, pages 10684–10695, 2022.
- [38] Soumik Mukhopadhyay, Matthew Gwilliam, Vatsal Agarwal, Namitha Padmanabhan, Archana Swaminathan, Srinidhi Hegde, Tianyi Zhou, and Abhinav Shrivastava. Diffusion models beat gans on image classification. *arXiv preprint arXiv:2307.08702*, 2023.
- [39] Zhiqing Sun and Yiming Yang. Difusco: Graph-based diffusion solvers for combinatorial optimization. *Advances in neural information processing systems*, 36:3706–3731, 2023.
- [40] Jingwei Liu, Ling Yang, Hongyan Li, and Shenda Hong. Retrieval-augmented diffusion models for time series forecasting. *Advances in Neural Information Processing Systems*, 37:2766–2786, 2024.
- [41] Zihao Wang. Score-based generative modeling through backward stochastic differential equations: Inversion and generation. *arXiv preprint arXiv:2304.13224*, 2023.
- [42] Zijun Long, Kangheng Liang, Gerardo Aragon Camarasa, Richard Mccreadie, and Paul Henderson. Diffusion augmented retrieval: A training-free approach to interactive text-to-image retrieval. In *Proceedings of the 48th International ACM SIGIR Conference on Research and Development in Information Retrieval*, pages 823–832, 2025.
- [43] Julien Guinot, Elio Quinton, and György Fazekas. Gd-retriever: Controllable generative text-music retrieval with diffusion models. *arXiv preprint arXiv:2506.17886*, 2025.
- [44] Lingkai Kong, Yuanqi Du, Wenhao Mu, Kirill Neklyudov, Valentin De Bortoli, Dongxia Wu, Haorui Wang, Aaron Ferber, Yi-An Ma, Carla P Gomes, et al. Diffusion models as constrained samplers for optimization with unknown constraints. *arXiv preprint arXiv:2402.18012*, 2024.
- [45] Luke Snow and Vikram Krishnamurthy. Finite-sample bounds for adaptive inverse reinforcement learning using passive langevin dynamics. *IEEE Transactions on Information Theory*, 2025.
- [46] Yadong Zhang, Siyu Lu, Qiang Liu, and Xingxing Wang. Diffuretrieval: A chain-of-thought enhanced diffusion retrieval in sponsored search. In *Companion Proceedings of the ACM Web Conference 2024*, pages 533–536, 2024.
- [47] Raoul Kalisvaart, Masoud Mansoury, Alan Hanjalic, and Elvin Isufi. Towards carbon footprint-aware recommender systems for greener item recommendation. *ACM Transactions on Recommender Systems*, 2025.
- [48] Harris Scells, Shengyao Zhuang, and Guido Zuccon. Reduce, reuse, recycle: Green information retrieval research. In *Proceedings of the 45th International ACM SIGIR Conference on Research and Development in Information Retrieval*, pages 2825–2837, 2022.
- [49] Xiangzhong Luo, Di Liu, Hao Kong, Shuo Huai, Hui Chen, and Weichen Liu. You only search once: On lightweight differentiable architecture search for resource-constrained embedded platforms. In *Proceedings of the 59th ACM/IEEE Design Automation Conference*, pages 475–480, 2022.
- [50] Xiangzhong Luo, Di Liu, Hao Kong, Shuo Huai, Hui Chen, and Weichen Liu. Surgenas: A comprehensive surgery on hardware-aware differentiable neural architecture search. *IEEE Transactions on Computers*, 72(4):1081–1094, 2022.
- [51] Lianming Huang, Shangyu Wu, Yufei Cui, Ying Xiong, Xue Liu, Tei-Wei Kuo, Nan Guan, and Chun Jason Xue. Raee: A robust retrieval-augmented early exiting framework for efficient inference. *arXiv preprint arXiv:2405.15198*, 2024.
- [52] Liang Liu, Mingzhu Shen, Ruihao Gong, Fengwei Yu, and Hailong Yang. Nnlqp: A multi-platform neural network latency query and prediction system with an evolving database. In *Proceedings of the 51st International Conference on Parallel Processing*, pages 1–14, 2022.
- [53] Max Welling and Yee W Teh. Bayesian learning via stochastic gradient langevin dynamics. In *Proceedings of the 28th international conference on machine learning (ICML-11)*, pages 681–688, 2011.
- [54] Eric Jang, Shixiang Gu, and Ben Poole. Categorical reparameterization with gumbel-softmax. *arXiv preprint arXiv:1611.01144*, 2016.

- [55] Hongyu Ke, Wanxin Jin, and Haoxin Wang. Carboncp: Carbon-aware dnn partitioning with conformal prediction for sustainable edge intelligence. *arXiv preprint arXiv:2404.16970*, 2024.
- [56] Ting Chen, Simon Kornblith, Mohammad Norouzi, and Geoffrey Hinton. A simple framework for contrastive learning of visual representations. In *International conference on machine learning*, pages 1597–1607. PmLR, 2020.
- [57] Payal Bajaj, Daniel Campos, Nick Craswell, Li Deng, Jianfeng Gao, Xiaodong Liu, Rangan Majumder, Andrew McNamara, Bhaskar Mitra, Tri Nguyen, et al. Ms marco: A human generated machine reading comprehension dataset. *arXiv preprint arXiv:1611.09268*, 2016.
- [58] Joel Mackenzie, Andrew Trotman, and Jimmy Lin. Efficient document-at-a-time and score-at-a-time query evaluation for learned sparse representations. *ACM Transactions on Information Systems*, 41(4):1–28, 2023.
- [59] Antonio Mallia, Michal Siedlaczek, Joel Mackenzie, and Torsten Suel. Pisa: Performant indexes and search for academia. *Proceedings of the Open-Source IR Replicability Challenge*, 2019.
- [60] Stephen Robertson, Hugo Zaragoza, et al. The probabilistic relevance framework: Bm25 and beyond. *Foundations and trends® in information retrieval*, 3(4):333–389, 2009.
- [61] Colin Raffel, Noam Shazeer, Adam Roberts, Katherine Lee, Sharan Narang, Michael Matena, Yanqi Zhou, Wei Li, and Peter J Liu. Exploring the limits of transfer learning with a unified text-to-text transformer. *Journal of machine learning research*, 21(140):1–67, 2020.
- [62] Shengyao Zhuang and Guido Zuccon. Fast passage re-ranking with contextualized exact term matching and efficient passage expansion. *arXiv preprint arXiv:2108.08513*, 2021.
- [63] Antonio Mallia, Omar Khattab, Torsten Suel, and Nicola Tonellotto. Learning passage impacts for inverted indexes. In *Proceedings of the 44th International ACM SIGIR Conference on Research and Development in Information Retrieval*, pages 1723–1727, 2021.
- [64] Luyu Gao, Zhuyun Dai, Tongfei Chen, Zhen Fan, Benjamin Van Durme, and Jamie Callan. Complement lexical retrieval model with semantic residual embeddings. In *European Conference on Information Retrieval*, pages 146–160. Springer, 2021.
- [65] Thibault Formal, Carlos Lassance, Benjamin Piwowarski, and Stéphane Clinchant. Splade v2: Sparse lexical and expansion model for information retrieval. *arXiv preprint arXiv:2109.10086*, 2021.

A Appendix: Theoretical Proofs

A.1 Convergence of Retrieval-Guided Langevin

Theorem A.1. Let $U : \mathbb{R}^n \rightarrow \mathbb{R}$ be L -smooth and m -strongly convex. Assume for every query q the map $z \mapsto V(q, z)$ has L_V -Lipschitz gradient and

$$D := \sup_{q,z} \|\nabla_z V(q, z)\| < \infty. \quad (21)$$

Consider the discrete update

$$z_{t+1} = z_t - \gamma_1 \nabla_z U(D(z_t)) + \gamma_2 \nabla_z V(q, z_t) + \sqrt{2\gamma_3} \xi_t, \quad (22)$$

where $\{\xi_t\}$ are i.i.d. $\mathcal{N}(0, I)$ and $\gamma_1, \gamma_2, \gamma_3 > 0$ satisfy $\gamma_1 + \gamma_2 \leq 1/(4L)$. Then for all $t \geq 0$

$$\mathcal{W}_2(\mu_t, \pi) \leq \left(1 - \frac{m\gamma_3}{2}\right)^t \mathcal{W}_2(\mu_0, \pi) + \frac{3\gamma_2 L_V D}{m}, \quad (23)$$

where μ_t is the law of z_t and $\pi \propto e^{-U/\gamma_3}$.

where \mathcal{W}_2 denotes the 2-Wasserstein distance, $D(z)$ is the decoder mapping, L and m are smoothness/strong-convexity constants of U , L_V is the Lipschitz constant of $\nabla_z V$, and D is defined in (21). Use a synchronous coupling: run two chains $\{z_t\}, \{z'_t\}$ with the same noises ξ_t . Subtract updates and apply the triangle inequality to obtain

$$\|z_{t+1} - z'_{t+1}\| \leq \|z_t - z'_t - \gamma_1(\nabla U(D(z_t)) - \nabla U(D(z'_t)))\| + \gamma_2 L_V \|z_t - z'_t\|. \quad (24)$$

where we used $\|\nabla_z V(q, z_t) - \nabla_z V(q, z'_t)\| \leq L_V \|z_t - z'_t\|$. By m -strong convexity and L -smoothness of U (and suitable choice of γ_1, γ_3) there exists $\alpha = \frac{m\gamma_3}{2} \in (0, 1)$ such that

$$\|z_t - z'_t - \gamma_1(\nabla U(D(z_t)) - \nabla U(D(z'_t)))\| \leq (1 - \alpha)\|z_t - z'_t\|. \quad (25)$$

Combining (24)–(25) yields one-step contraction $\|z_{t+1} - z'_{t+1}\| \leq (1 - \alpha + \gamma_2 L_V)\|z_t - z'_t\|$. Treating $\gamma_2 \nabla_z V$ as a bounded perturbation with amplitude $\gamma_2 D$ and unrolling the recursion gives geometric decay up to an additive steady-state term bounded by $O(\gamma_2 L_V D/m)$. Translating the coupling bound to \mathcal{W}_2 yields (23). \square

A.2 Unbiasedness and Covariance of EW-RLS

Consider the linear model $y_t = x_t^\top \theta^* + \eta_t$ with zero-mean independent noise η_t having sub-Gaussian proxy σ^2 . The EW-RLS recursions are

$$K_t = P_{t-1} x_t (\lambda + x_t^\top P_{t-1} x_t)^{-1}, \quad (26)$$

$$\theta_t = \theta_{t-1} + K_t (y_t - x_t^\top \theta_{t-1}), \quad (27)$$

$$P_t = \lambda^{-1} (P_{t-1} - K_t x_t^\top P_{t-1}). \quad (28)$$

where $\lambda \in (0, 1)$ is the forgetting factor.

Proposition A.2. *If $\mathbb{E}[\theta_0] = \theta^*$ then for all t the estimator is unbiased: $\mathbb{E}[\theta_t] = \theta^*$. Moreover*

$$\mathbb{E}\|\theta_t - \theta^*\|^2 = \sigma^2 \text{tr}(P_t), \quad (29)$$

and under $\|x_t\|^2 \leq B_x$ and $\text{tr}(P_0) \leq T_0$ we have

$$\mathbb{E}\|\theta_t - \theta^*\|^2 \leq \sigma^2 \left(\lambda^t T_0 + \frac{dB_x}{1 - \lambda} \right). \quad (30)$$

where $\text{tr}(\cdot)$ is the matrix trace, d is parameter dimension, B_x bounds regressor norm, and T_0 bounds $\text{tr}(P_0)$. Taking expectation in (27) and using $\mathbb{E}[\eta_t] = 0$ yields $\mathbb{E}[\theta_t] = \mathbb{E}[\theta_{t-1}]$ when $\mathbb{E}[\theta_{t-1}] = \theta^*$, hence unbiasedness by induction. Define $e_t = \theta_t - \theta^*$; standard RLS algebra gives $\mathbb{E}[e_t e_t^\top] = \sigma^2 P_t$, so (29) holds. From (28) one can show the scalar recursion $\text{tr}(P_t) \leq \lambda \text{tr}(P_{t-1}) + dB_x$; iterating yields the bound in (30). \square

A.3 Quantization Error Bound

Let g_U be the exact gradient and \tilde{g}_U its uniform 8-bit quantization with step Δ . Uniform rounding implies

$$\|\tilde{g}_U - g_U\|_\infty \leq \frac{\Delta}{2}, \quad (31)$$

where $\|\cdot\|_\infty$ is the maximum absolute coordinate error. Assuming the carbon surrogate \hat{C} is Lipschitz in the gradient with sensitivity coefficients k_M, k_F applied to operation-count vectors Mop, Flop, a first-order bound gives

$$|\hat{C}_{\text{quant}} - \hat{C}| \leq \frac{\Delta}{2} (k_M \|\text{Mop}\|_1 + k_F \|\text{Flop}\|_1), \quad (32)$$

where $\|\cdot\|_1$ is the vector 1-norm. For $\Delta \leq 8 \times 10^{-4}$ this evaluates below 0.05 g CO₂ in our workloads. For recall, let $s_{(K)}$ and $s_{(K+1)}$ be the K -th and $(K+1)$ -th exact scores; define $\Delta_{\text{margin}} = s_{(K)} - s_{(K+1)}$. If per-item score perturbation obeys $\max_i |\tilde{s}_i - s_i| \leq \delta < \Delta_{\text{margin}}/2$ then top- K is unchanged. Combining a model-dependent constant C_s with (31) gives $\max_i |\tilde{s}_i - s_i| \leq C_s \Delta/2$; thus if $C_s \Delta/2 < \Delta_{\text{margin}}/2$ recall is preserved. Empirically for our tasks $\Delta \leq 8 \times 10^{-4}$ yields recall drop within 0.3%. \square